

# Rupture Dynamics and Chromatin Herniation in Deformed Nuclei

Dan Deviri,<sup>1,\*</sup> Dennis E. Discher,<sup>2</sup> and Sam A. Safran<sup>1</sup>

<sup>1</sup>Department of Materials and Interfaces, Weizmann Institute of Science, Rehovot, Israel and <sup>2</sup>Molecular and Cell Biophysics Lab, University of Pennsylvania, Philadelphia, Pennsylvania

**ABSTRACT** During migration of cells *in vivo*, in both pathological processes such as cancer metastasis or physiological events such as immune cell migration through tissue, the cells must move through narrow interstitial spaces that can be smaller than the nucleus. This can induce deformation of the nucleus which, according to recent experiments, may result in rupture of the nuclear envelope that can lead to cell death, if not prevented or healed within an appropriate time. The nuclear envelope, which can be modeled as a double lipid bilayer attached to a viscoelastic gel (lamina) whose elasticity and viscosity primarily depend on the lamin composition, may utilize mechanically induced, self-healing mechanisms that allow the hole to be closed after the deformation-induced strains are reduced by leakage of the internal fluid. Here, we present a viscoelastic model of the evolution of a hole nucleated by deformations of the nuclear lamina and estimate the herniation of chromatin through the hole and its relation to the lamin expression levels in the nuclear envelope.

## INTRODUCTION

The nucleus of animal cells, which contains the genetic material of the cell in its interior nucleoplasm, is the largest organelle in the cells, with a typical radius of  $\sim 3 \mu\text{m}$  in mammalian cells (1,2), and occupies  $\sim 10\%$  of the total cell volume (3). The nucleoplasm includes DNA organized into chromatin, dispersed in a small molecule (water/protein/enzyme) solution, which is bounded by the nuclear envelope (NE), comprised of a two-bilayer membrane separated by a volume termed the “perinuclear space”. The inner nuclear membrane (INM) is connected to a viscoelastic, dense network of intermediate filament proteins mostly comprising the A- and B-type lamins (the lamina). The INM and the outer nuclear membrane are connected by many nuclear pore complexes (NPCs), containing proteins sometimes modeled as polymer brushes grafted to the inside of cylindrical tubes (4), which results in a protein-covered channel of 50 nm diameter that connects the cytoplasm and the nucleoplasm. The NPC regulates the essential transport of proteins, RNA molecules, and other small ions and molecules to and from the nucleus (5,6); this maintains a controlled environment in the nucleoplasm, distinguished from the cytoplasm, which is essential for

proper function of the cell. Because the function of the NE is essential for the survival of the cell, a pathological event that impairs the integrity of the NE may cause an unregulated loss of genetic material and thus lead to cell death.

Recent experiments (7) have shown that motile cells placed on a perforated plate deform as they migrate (within 24 h) from the upper to the lower regions of the plate. However, the migrating cells show a marked reduction in their survival rate as they traverse pores that are smaller than their nucleus size. By using A-type lamin partial knockout cells, it was shown that the survival rate was dependent on the A-type lamin content of the nuclear lamina, which is attached to the INM (8); similar results were obtained in A-type lamin knockout cells subjected to cyclic mechanical strain (9). The composition of the lamina network affects the viscoelastic properties of the NE and the nucleus (10,11), whose rheology obeys power-law scaling: behaving elastically at short times and as a fluid at long times, with no single timescale separating the two regimes (12,13). Migration of cells through narrow constrictions, both *in vitro* (microfluidic channels) and *in vivo* (3D collagen networks), may impair the integrity of the NE, resulting in unregulated exchange of cytoplasmic and nucleoplasmic proteins and DNA double-strand breaks, with a probability that increases with decreasing constriction cross section (14,15). Rupture of the NE has not yet been directly imaged in the recently published studies

Submitted January 23, 2017, and accepted for publication July 20, 2017.

\*Correspondence: dan.deviri@weizmann.ac.il

Editor: Cecile Sykes.

<http://dx.doi.org/10.1016/j.bpj.2017.07.014>

© 2017 Biophysical Society.

and is inferred through observations of the exchange of nucleoplasmic and cytoplasmic proteins (7,14–17). Our predictions for rupture and healing can so far only be correlated with evidence for protein exchange. Evidence of rupture is not unique to migration assays and has also been observed in nuclei squeezed between two parallel surfaces (18). These observations imply that rupture of the NE may be generically caused by deformation-induced, lateral strains and stresses, whose experimental origins may be different. In migration assays, when the constriction dimensions are smaller than the radius of the nucleus, the nucleus must deform for the cells to fit the constriction and migrate. Even in vivo, the NE can support pressure gradients that arise during migration (19); we therefore expect that for relatively small deformations, in the absence of holes, the flow of fluid outside of the nucleus through the NPC must be small so that the nuclear volume is approximately conserved. Shear deformation (deformation that keeps the volume constant) of the undeformed, approximately spherical nucleus in its undeformed state, as shown in Fig. 1 A, increases the area of the NE; such area increase results in elastic stretch that leads to surface tensions and strains, which can eventually cause rupture. Interestingly, DNA damage was observed in migrating cells even in the absence of rupture; the damage may be caused by changes in the nucleoplasmic, spatial concentration profile of chromatin that sequester repair enzymes and other essential factors from regions of high chromatin density (16,20).

Understanding and controlling rupture dynamics in vesicles is important for many areas of science, engineering, and medicine such as drug delivery (21), antimicrobial peptides (22), membrane fusion (23), and DNA delivery (24). Due to the importance of the problem, extensive research has been conducted regarding the nucleation and dynamics of pores in fluid, lipid membranes, both in flat membranes (25,26) and in closed vesicles (27–34). However, this body of knowledge disregards the special characteristics of the nucleus, such as its complex internal fluid and viscoelastic membrane. As a result, although migration of cells through interstitial pores in the extracellular matrix is a key characteristic of many biological processes both physiological (embryogenesis, white blood cell migration, wound healing,

etc.) and pathological (cancer metastasis or tissue invasion), the mechanism that protects these cells during migration and its fundamental origin is still not well understood.

Measurements of hole formation, growth, and healing, have previously been performed in the context of lipid bilayer vesicles that contain homogenous aqueous solutions. The surface tension was induced not by passage through narrow pores, but by laser tweezers (35) or adhesion (27) (topological changes). In addition, and most importantly, the membrane and internal liquid were fluid in nature and not viscoelastic. A leading hydrodynamic theoretical work on the subject formulated equations describing the dynamics of hole growth and closing coupled to internal fluid leak-out (27,28); numerical solutions of the equations over a wide range of parameters indicated different regimes of the dynamics. In addition, analytical and scaling arguments explaining some of these regimes were presented. Although these studies gave insights into hole formation and dynamics and indeed introduced the concept of outflow of fluid as a controlling factor in hole formation, they were performed in the context of viscous, fluid-filled, lipid vesicles whose properties are different from the NE and chromatin network (36).

The majority (90%) of migration-induced NE rupture events are preceded or coincide with formation and eventual disappearance (probably due to bursting) of nuclear membrane blebs (14). Protein complexes associated with damage response (to bilayers, i.e., ESCRT III proteins that promote bilayers healing and to chromatin, i.e., 53BP1 that binds double-stranded breaks) are recruited after bleb bursting (15). This points to the role of blebs as membrane hole nucleation sites that can then lead to chromatin damage. Disruption of the lamina network, either by lamin knock-down or due to mutations, is positively correlated with the formation of blebs, abnormal nuclear morphology, or impaired nuclear mechanics (18,37,38). This implies a possible mechanistic relation between the integrity of the nuclear lamina and the formation of blebs and subsequent bursting. In this work, we focus on the physics of laminar hole formation and healing, which we assume to be controlled by flow of the lamina; we hypothesize that laminar hole nucleation is an essential first step that must

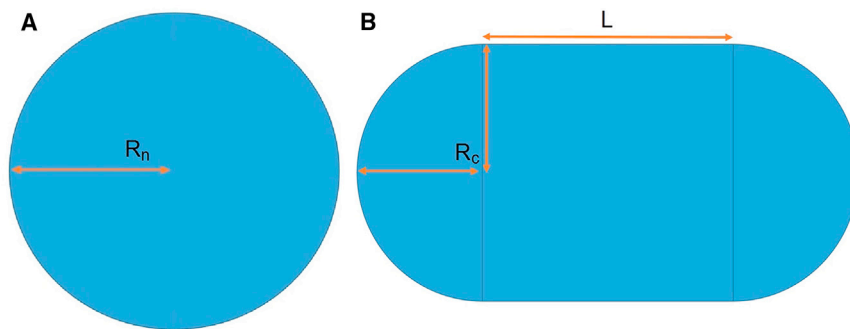


FIGURE 1 Models of the nuclear shape. (A) Undeformed state: here we have a sphere of radius  $R_n$  and surface area  $A_u$ . (B) Deformed state: here we show a cylinder of length  $L$  and radius  $R_c$  (which equals the cross-sectional radius of the constriction when  $R_c < R_n$ ) with two hemispherical caps; the total surface area of the deformed state is  $A_d$ . Conservation of the volume of the nucleus determines the length  $L$  via the relation  $4\pi R_n^3/3 = 4\pi R_c^3/3 + \pi R_c^2 L$ . From this, one can find the total area  $A_d$  of the deformed nucleus as a function of the constriction cross-sectional radius  $R_c$ . To see this figure in color, go online.

precede and then lead to bleb formation, which persists until the laminar hole is healed. However, the physics of bleb formation and bursting is outside the scope of this article, which focuses on lamina hole dynamics/healing and its role in facilitating chromatin extrusion. Our theory thus focuses on the dynamics of rupture in the lamina, which is a crucial first step that precedes bleb formation.

Upon deformation, the internal pressure in the nucleus increases due to the compressive forces exerted on the nucleoplasm. In regions where no external forces are exerted (such as the leading edge), the increased pressure is equilibrated via the Laplace law by the surface tension of the NE. Therefore, the presence of a hole in the lamina (but not the membranes) disrupts the mechanical force balance near the hole. This may lead to fluid outflow from the nucleus that inflates the bilayers in the vicinity of the hole, leading to the formation of a bleb. Once this happens, chromatin normally found in the nucleus can herniate through the lamina hole and then reside in the bleb (14,18). If the bleb bursts, the chromatin may then be damaged due to its exposure to the chemical environment of the cytoplasm. We theoretically predict the dynamics of the lamina ruptures and suggest their biological significance. The molecular properties enter in parameters such as the hole line tension, i.e., lamina 2D Young's modulus  $E$  and viscosity  $\eta$ , and the local chromatin-dependent viscosity of the nucleoplasm. (Note that whereas we regard the lamina as compressible within its plane, it is indeed incompressible in three dimensions when its finite thickness is taken into account—namely, stretching in plane leads to a reduction in thickness.)

The theory in this article comprises two subsections: In the first, we formulate and solve what is, to the best of our knowledge, a novel hydrodynamic theory that may describe the postnucleation evolution of the hole radius and lateral strain in the nuclear lamina modeled as a deformed, viscoelastic shell that contains a fluid-filled gel network (as a model of the nucleoplasm) on its lumen side. We analyze this theory analytically in two limits: one in which the deformation-induced strain is relaxed mainly due to outflow; and the other in which strain reduction is mainly due to hole growth. In the second subsection, which is most relevant for the biological problem of chromatin damage, we predict the relative amount of chromatin that herniates through the hole and resides within the forming bleb, as a function of the viscoelastic properties of the lamina. This connects the rupture dynamics predicted by our model and others (28) to biological, rupture-induced damage. Relating the viscoelastic properties of the lamina to the expression of lamins allows prediction of the optimal expression required to prevent significant chromatin herniation, thus optimizing survivability during migration as expected (to some extent) *in vivo*. These subsections are followed by a discussion that links the theoretical predictions to experimental observation and proposes future experiments to quantitatively test our ideas.

## MATERIALS AND METHODS

The theoretical methods of elasticity and hydrodynamics were used to calculate the rupture and healing properties of the lamina. These are detailed in the [Supporting Material](#).

### Physical background

The viscoelastic properties of the NE are primarily determined by the nuclear lamina (10,11,13). Various experiments have measured the relative contributions of the different lamin proteins to the mechanical properties of the NE (10,11,37). However, the roles of the different lamins is not yet a matter of consensus, because the varying results and conclusions may depend on the experimental method and the timescales of measurements. In the following sections, where we present and solve the theoretical model, all the predictions are expressed only in terms of the viscosity and 2D Young's modulus of the nuclear envelope. At this level, the theory is generic in nature; the relation between the viscoelastic parameters and the molecular compositions to lamin expression is outside the scope of the theory and must be determined from experiment.

The physics governing area changes in lipid bilayers, which are typically  $\sim 4$  nm thick (39), is determined by the joint contribution of the elastic forces due to the decrease in the 2D density of lipid molecules (40) and the entropic forces due to suppression of the membranes' thermal undulations (26). Bending moduli of membranes scale as a power law of the membrane thickness (between 2 and 3) (41,42). Because the NE comprises two lipid bilayers and a lamina that is  $\sim 14$  nm thick (43), it is at least sixfold thicker than lipid bilayers (and may be even thicker because the two lipid bilayers are spaced), and thus has a much larger bending modulus. This effectively suppresses the thermal undulation of the NE and its components and enables the use of purely mechanical, linear elastic constitutive laws when describing the lamina.

Hole formation in flat, tensed membranes, whose molecular area density is lower than its value in a relaxed membrane, results in two opposing contributions to the energy of the membrane: In the first, the hole lowers the membrane energy proportional to its area, due to dispersion, in the rest of the membrane, of the lipid molecules that were originally in the area of the hole. This increases the area density of molecules closer to their equilibrium value and thus reduces the surface deformational energy. In the second, the hole increases the membrane energy in a manner proportional to the hole circumference due to the energy associated with the line tension (29). Line tension promotes hole healing and arises due to the bending energy costs of curving the lipid leaflets on a scale of the order of their thickness, required to eliminate hydrophilic-hydrophobic contact at the circumference of the hole. The competition between line tension and surface tension determines a critical nucleation radius that depends on the deformation-induced surface tension of the membrane; holes smaller than the critical radius will close whereas larger holes will grow up to a characteristic radius (this radius can be metastable (27)). In vesicles comprising only a single lipid bilayer, the time required for the hole formation/healing cycle is of the order of seconds (28), which is much faster than the timescales of migration and rupture measured in migration-induced nuclear rupture (14). Experiments have not yet directly imaged nuclear rupture; so far, existence of rupture was inferred from leakage of nuclear proteins such as GFP-NLS into the cytoplasm (7,14,15,17). Measurements of the time evolution of cytoplasmic fluorescent signal after rupture suggest that the healing of the ruptures occurs on the scale of a few tens of minutes (14,15,17). This time is greatly increased (approximately doubled) by the disruption of the ESCRT III system (15), which indicates its role in the healing of holes in the bleb.

Because the NE contains a variety of integral proteins which, in a coarse-grained picture, can be thought of as defects in a homogeneous viscoelastic layer, it is reasonable to assume that the hole nucleated at such a defect site, such as the NPC. Because the microscopic details of the nucleation are unknown, we consider the growth of a hole whose initial radius is larger

than the critical nucleation radius, and define  $R_i$  as the initial hole radius, taken to be 25 nm, of the order of the NPC channel size (5).

The qualitative features of the elastic response of shells, such as the NE, to deformations depends on whether the shells are closed (lack holes with free boundaries) or open (contain holes with free boundaries). Whereas in open shells the boundary of the hole is free to move to reduce the lateral strains, this is not the case in closed shells. Therefore, in open shells, the main contribution to the deformation energy originates in bending of the shell, whereas in closed shells the deformation results in global, in-plane strains (42). Bending involves much smaller deformation energies compared with in-plane strains so that the only large strains in an open shell are those in the direct vicinity of the hole, which cause its growth. In the case of an intact NE, the rigid protein ring formed by NPC can be modeled as a hole with fixed boundaries that cannot relax the imposed surface tension by their motion. Therefore, in its intact state, the NE behaves as a closed shell that is strained (in-plane) over its entire area. On the other hand, rupture of the NE (with the creation of a hole whose size is significantly larger than that of the NPC) creates free boundaries that can adjust to the imposed surface tensions by their motion so that the NE can be modeled as an open shell, in which the lateral strains are concentrated only in the vicinity of the hole. For this reason, we consider only single and not multiple holes in the NE.

Closed surfaces, such as vesicles or the NE, express mechanical equilibrium via the Young-Laplace relation that states that the product of their curvature and surface tension is equal to half the pressure difference between the two sides of the surface. However, once a hole is formed in an otherwise closed membrane, these initial pressure differences lead to an outflow of internal fluid through the hole. This outflow reduces the total area of the surface and hence the packing area per molecule and the surface tension. When the packing area is reduced to its equilibrium packing area that minimizes the membrane free energy value (in the absence of external stress), the surface tension vanishes and along with it, the pressure difference. Previous experiments on the rupture of vesicles, have shown that the two competing mechanisms of surface tension relief (hole growth) and total area reduction (outflow of internal fluid) cause the hole to shrink after an initial period of growth and eliminate the metastable state of the hole that exists in flat membranes (26,27).

However, the nucleoplasm is not a simple viscous fluid (44), and the relation between the flow and pressure gradient is therefore complex. In this article, the nucleoplasm is considered to be a (very) high concentration solution of chromatin fibers in a good solvent (water + small molecules; see Fig. 2 A). We model the chromatin as a semiflexible polymer with persistence length  $l_p$ . The persistence length of dsDNA in physiological conditions is  $\sim 50$  nm (45), and we assume that  $l_p > 50$  nm due to higher level organization of dsDNA in chromatin fiber. The rheology of the nucleoplasm is considered in two extreme limits, one in which only the aqueous phase can flow (see Fig. 2 B) and another, in which both the chromatin and the aqueous phase flow together (see Fig. 2 C). Particle nanotracking

experiments have measured an effective, coarse-grained, kinematic viscosity of nucleoplasm that is more than three orders-of-magnitude larger than the kinematic viscosity of water (44), implying that the joint flow of the chromatin and the aqueous phase is considerably more viscous than that of the aqueous phase alone.

## RESULTS

### Rupture and healing dynamics

In this subsection, we formulate and solve a theory for the coupled dynamics of hole growth/healing of a deformed viscoelastic shell (as a model of the nuclear envelope) and the resulting outflow of a high concentration solution of semiflexible polymer in a good solvent (as a model of chromatin; see Fig. 2 A). We consider the postnucleation dynamics of a hole that has been nucleated at a defect site in the shell. High curvature regions in the deformed shell are characterized by higher bending energy; thus, nucleation of holes in regions of high curvature is thermodynamically favorable. We therefore suggest that, for the case of migration-induced deformation, a probable nucleation site of the hole is in the leading edge of the migrating shell because it is characterized by relatively high curvature. Whereas the flow of the solvent phase alone is characterized by a kinematic viscosity  $\eta_s$ , the effect of the semiflexible polymer (which can spatially rearrange during outflow due to friction with the solvent phase) on the rheology of the solution has not yet been elucidated. The friction between the solvent phase and the semiflexible polymer impedes the outflow of the aqueous phase in a manner that may depend on many details.

To account for the unknown, complex effect of the semiflexible polymer on the solvent phase outflow, we consider two very different and simple limiting-case models for the rheology of the solution in our calculations of hole growth and closure. In the first, we consider a scenario in which the semiflexible polymers rearrange such that a channel is formed in between regions where the semiflexible polymers are more densely packed and solvent phase flow is greatly reduced (see Fig. 2 B). This channel serves as a conduit

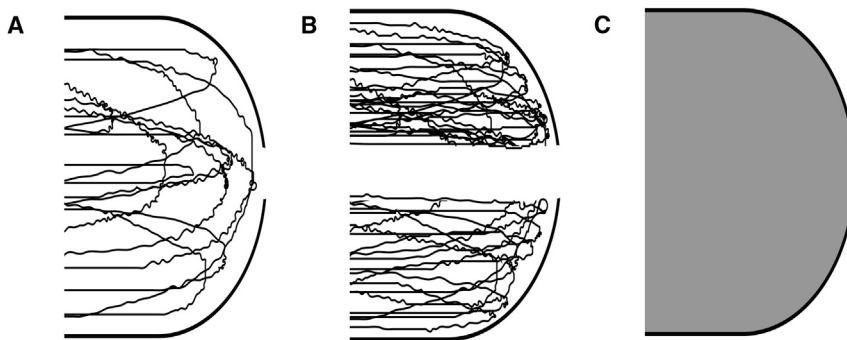


FIGURE 2 Models for chromatin organization and aqueous phase flow. (A) Shown here is a high concentration of semiflexible polymer (as a model of chromatin) in a good solvent (water + molecules); the rheology of this model is complex because the polymer chains can rearrange as the solvent phase flows out of the nuclear volume via a hole in the nuclear envelope. (B) Limiting case model I: here, polymer chains rearrange (due to the solvent phase flow) to form a channel that serves as a conduit to the solvent phase outflow. The conduit has an effective radius of order of the hole radius  $R$  and effective contour length  $d^*$ . (C) Limiting case model II: here the polymer and solvent phases flow together and are coarse-grained as a homogenous viscous fluid of viscosity  $\eta_s^*$ .

that directs the flow of the solvent phase and therefore minimizes dissipation by reduction of the friction between the solvent phase and the semiflexible polymers. The flow in the conduit is modeled as a laminar flow in a cylinder (Hagen-Poiseuille flow) whose radius is set by the hole size that allows the solvent phase flow (which is the driving force for the rearrangements of the semiflexible polymers that result in the formation of the channel). The effective tube length can be much larger than the hole size. In the second model, we consider a coarse-grained model of the flow in which the semiflexible polymer phase and the solvent phase are lumped together as a homogenous, viscous fluid with an effective, kinematic viscosity that is much larger than the  $\eta_s$ , the kinematic viscosity of the solvent phase alone (see Fig. 2 C). The two models are very different from a physical perspective: in the first model, the semiflexible polymer phase rearranges but does not flow, so that it is distinct from the flowing solvent phase. In the second model, the semiflexible polymer and solvent phases flow together and are treated as a single, homogenous fluid. We show below that, although these two limiting-case models greatly differ, our qualitative predictions for the dependence of the hole growth/healing dynamics and the degree of deformation-induced, polymer extrusion on the viscoelastic properties of the shell are insensitive to which model is used.

Both cases result in similar dynamics that can be approximated by hole growth that increases exponentially with time, until the hole reaches a maximal radius  $R_m$ . This regime is followed by an approximately linear decrease of the hole size with time. The major differences between the two models result in different expressions for  $R_m$  and the velocity of hole closing (after it reaches its maximum) as functions of the viscoelastic properties of the shell. For this reason, we conclude that the dynamics of an exponential increase, followed by a linear decrease that is common to both models, is insensitive to the details of the effect of the semiflexible polymer phase on the rheology of the solution. We therefore predict that the experimental dynamics of the rupture are of the same form. Below, we show that the qualitative dependence of the amount of polymer that is extruded on the viscoelastic properties of the shell is also independent of the model used for the rheology of the solution. The biological consequences are explicated in the Discussion section at the end of the article, which may be relevant to the reduction in cell viability measured in experiments.

Before deformation and the resulting hole nucleation, the viscoelastic shell is regarded as impermeable and has the shape of a sphere with area  $A_u$  (see Fig. 1 A). When the spherical shell is deformed, the surface area of the shell increases (because a sphere has minimal area for a fixed volume), laterally stretching the shell. We treat the surface tensions and lateral strains by averaging over the entire area so that the initial strain,  $\epsilon_0$ , is proportional to the difference between the areas of the shell in the deformed and

undeformed states. (Before hole formation, the NE is approximately impermeable (46), so no outflow occurs.) We account for the rearrangements of the molecules in the shell by an approximately uniform lateral strain driven by the deformation; the timescale for molecular rearrangements in the shell is expected to be much faster than the time for hole growth/healing (tens of minutes), because hole growth/healing involves macroscopic displacements of molecules whereas the rearrangements involve only local displacements at the molecular scale.

Before a hole nucleates, the area of the deformed shell is denoted by  $A_d$ ; thus, the initial lateral strain  $\epsilon_0$  is given by the difference of the deformed and undeformed areas  $\epsilon_0 = (A_d - A_u)/A_u$ . In this article, for geometrical simplicity, we consider deformation of the shell due to forced migration through a constriction. Other deformation mechanisms (e.g., squeezing between plates or others), can in principle be modeled but we focus here on migration due to its biological ubiquity. For the constriction case, we model the deformed shell as a cylinder with two hemispherical caps whose radius is equal to that of the constriction (see Fig. 1 B). The geometry in Fig. 1 relates  $A_d$  to the constriction cross-sectional area  $A_c = \pi R_c^2$  by  $A_d = (1/3)(4A_c + A_u\sqrt{(A_u/A_c)})$ .

The hemispherical, laterally strained caps have smaller radii of curvature and larger surface tension than those of the initial, spherical nucleus. Stabilization of this larger curvature structure implies (via the Young-Laplace relation; Eq. 2) a larger pressure gradient across the shell compared with the initial, undeformed situation. Once a hole is formed, this pressure gradient gives rise to outflow of the solution from the inner side of the shell to the outer side. When hole nucleates, the solvent phase along with some semiflexible polymers flow out through the hole due to this pressure gradient. The importance of this outflow in hole dynamics was previously pointed out in the context of vesicle rupture (27). We note that local changes in the surface tension also contribute to the pressure difference, but our mean field model approximates the surface tension as uniform for the deformations of interest.

The lateral strain  $\epsilon$  resulting from the deformation-induced, increased shell area implies surface tension  $\sigma$ ; our model uses linear viscoelastic theory (applicable for shell rupture caused by lateral strains of a few percent) to relate the surface tension and lateral strain by  $\sigma = E\epsilon$ , where  $E$  is the 2D Young's modulus. If the shell is modeled as a Maxwellian, viscoelastic material, the dynamics of its flow and therefore of the hole growth/closing can be complex and dependent on the past configuration of the material. To simplify the problem, we approximate the dynamics of the shell to be solid-like at times that are shorter than the typical viscoelastic timescale  $\tau = \eta/E$ , where  $\eta$  is the surface viscosity of the shell (which is its kinematic viscosity multiplied by the shell thickness), and viscous fluidlike at times larger than  $\tau$ . In the solid regime, ignoring plastic

deformations that are usually not relevant for small strains, the material cannot flow, so that the hole radius does not change significantly (see [Supporting Material](#)). At times larger than  $\tau$ , the shell flows as a fluid and its dynamics can be calculated from force balance of the flow around a hole of radius  $R$  within a locally flat, viscous layer (see [Supporting Material](#)) (27):

$$\frac{dR}{dt} = \frac{1}{2\eta} R \left( \sigma - \frac{T}{R} \right). \quad (1)$$

[Equation 1](#) describes the time evolution of only the hole radius; to predict the full rupture dynamics, an equation for the evolution of the combined area  $A$  (defined to be the sum of the shell and the hole area) due to outflow, must be derived. The outflow is driven by a pressure difference  $\Delta p$  between the two sides of the shell;  $\Delta p$  is related to the surface tension by Young-Laplace law,

$$\Delta p = 2\sigma C, \quad (2)$$

where  $C = 1/R_c$  is the curvature in the vicinity of the hole (see [Fig. 1 B](#)). The relation between the flow rate  $Q$  of the solvent phase and the pressure difference  $\Delta p$  is different for the two models of the solution rheology considered; we now discuss each of them separately.

#### *Case I: solvent phase flow through a conduit formed by semiflexible polymers*

In the first case that we consider (see [Fig. 2 B](#)), the flow of the solvent phase is modeled as a flow through an effective cylindrical tube of radius  $R$  and length  $d^*$ , where the dissipation is due to the friction between the flowing solvent phase and the walls of a conduit of contour length  $d^*$ , bounded by a dense polymer region where solvent flow is strongly impeded. In this picture, the effective dissipation length  $d^*$  can be much larger than  $R$ , depending on the contour length of the conduit, which might be very tortuous, leading to  $d^*$  that can be greater even than the dimensions of the shell. In this subsection, we formulate and solve a hydrodynamic theory for the dynamics of hole growth and shrinking in the shell for Hagen-Poiseuille outflow.

In the low Reynolds number limit, the outflow is laminar, so that the flow rate  $Q$  is (47) (see [Supporting Material](#)):

$$Q = -\frac{R_c}{2} \frac{dA}{dt} = \frac{\pi \Delta p R^4}{8\eta_s d^*}, \quad (3)$$

where  $\Delta p$  is the pressure difference between the two sides of the shell,  $\eta_s$  is the viscosity of the solvent phase of the nucleoplasm, and  $A$  is the combined area of both the shell and the hole. [Equation 3](#) is accurate in the limit that  $d^* \gg R$  so that end effects can be neglected.

Substituting linear elasticity relation  $\sigma = E\varepsilon$  and [Eq. 2](#) into [Eqs. 1](#) and [3](#) leads to two coupled equations that describe the dynamics of the combined area of the shell and the local hole radius:

$$\frac{dR}{dt} = \frac{E R}{\eta} \left( \varepsilon - \frac{T}{E R} \right), \quad (4)$$

$$\frac{dA}{dt} = -\frac{E}{2\eta_s d^*} \frac{\pi^2 R^4}{A_c} \varepsilon. \quad (5)$$

These equations show that the rate of change of the combined area is related to the hole radius by the outflow, whereas the rate of change of the hole radius is related to the lateral strain  $\varepsilon$  and the line tension  $T$ . (The strain is reduced from its initial value by the molecules donated to the shell due to the presence of the hole and by the area reduction due to outflow.)

To simplify the equations, we rescale the variables  $\tilde{R}$  and  $\tilde{A}$  to be of order unity, i.e.,  $\tilde{R} = R/R_i$ ,  $\tilde{A} = A/A_u$ , and  $\tilde{t} = t/\tau$ , where  $\tau = \eta/E$  and  $R_i$  is the initial radius of the hole directly after nucleation. Then, to account for more physical variables, we replace the variable  $\tilde{A}$  that appears in [Eq. 5](#) with the lateral strain, which results in the simplified, approximated form (see [Supporting Material](#)):

$$\frac{d\tilde{R}}{d\tilde{t}} = \frac{1}{2} \tilde{R} \varepsilon - \frac{\beta}{2}, \quad (6)$$

$$\frac{d\varepsilon}{d\tilde{t}} = -\left( 1 + \frac{2\rho\tilde{R}^2}{\delta} \right) \rho\tilde{R}^2 \varepsilon + \rho\tilde{R}\beta, \quad (7)$$

where  $\varepsilon = (A - \pi R^2 - A_u)/A_u = \tilde{A} - \rho\tilde{R}^2 - 1$  is the dimensionless, small lateral strain; and  $\beta$ ,  $\rho$ , and  $\delta$  are small, dimensionless parameters equal to  $(T/ER_i)$ ,  $(\pi R_i^2/A_u)$ , and  $(\eta_s d^*/\eta)$ , respectively (see [Supporting Material](#)). Henceforth we omit the tilde signs and write  $R$ ,  $A$ , and  $t$ .

The dynamical [Eqs. 6 and 7](#) are highly nonlinear and cannot be fully solved analytically. However, some general observations can still be made concerning the dynamics. First  $\varepsilon$ , which is initially positive, cannot become negative because if  $\varepsilon$  approaches zero, the derivative in [Eq. 7](#) is dominated by the positive term  $\rho\beta R$ , which then increases  $\varepsilon$ . Second, the hole will grow ( $(dR/dt) > 0$ ) up to a maximal size  $R_m$  that satisfies  $R\varepsilon = \beta$  at the time for which  $R = R_m$  as dictated by [Eq. 6](#). Hole growth and outflow decrease  $\varepsilon$  until it reaches its minimal value (which is shortly after  $R = R_m$ ), because hole closing increases the lateral strain and decreases the outflow. For the minimal strain, the derivative in [Eq. 7](#) is zero and so  $\varepsilon_{\min} = (\beta/(1 + (2\rho R^2/\delta)))R$ , and the rate of hole closing is then equal to  $(dR/dt) = (\beta/2)/(1 + (2\rho R^2/\delta)) - (\beta/2) \approx -(\beta/2)((2\rho R^2/\delta) \gg 1$  for  $R \sim R_m$ ; see [Supporting Material](#)), according to [Eq. 6](#).

During hole closing, the lateral strain increases due to the increase of the area outside the hole, which is now occupied by a lower density of molecules because some of those have returned to the previously larger hole. However, that effect is mitigated by outflow from the inner side of the shell that keeps the lateral strain small. If that outflow is large enough, the strain can be maintained at negligibly small values so that Eq. 6 predicts that the hole radius decreases linearly with time. When the effective dissipation length is too high, the outflow is too small to mitigate the growth of the lateral strain by hole closing ( $\rho\beta R$  is not small compared to  $-2\rho^2/\delta R^4\epsilon$  in Eq. 7), which in turn slows the rate of hole radius decrease. The hole closing rate then returns to the value of  $-\beta/2$  when the hole is small enough, because  $1/2 Re$  will again be negligible compared with  $-\beta/2$  in Eq. 6. Numerical solutions of the equations for a wide range of effective dissipation lengths verify our predictions of the late-time behavior of the hole radius (see Fig. 3).

At early times, before the hole radius reaches its maximal value and then decreases linearly with time, the dynamics is complex and more sensitive to the model parameters. However, one can still qualitatively explain the behavior at early

times in two limits: 1) fast, outflow-induced strain relaxation compared with hole growth-induced strain relaxation, and 2) for the opposite case. In limit 1, the strain is quickly relieved by outflow whereas the hole size remains approximately constant (or grows very slowly). In that case, the hole radius decreases very soon after the hole forms. In the opposite case of slow outflow (limit 2), the shell combined area is approximately constant as the hole radius increases (due to the surface tension). At early times, when the lateral strain is approximately constant and the constant term in Eq. 6 is negligible, this equation predicts exponential growth of the hole radius as a function of time (28); this can be derived analytically from Eqs. 4 and 5 (see the Supporting Material).

Our numerical analysis of the equations shown in Fig. 3 A demonstrates that due to the exponential growth, the maximal hole radius can be significantly greater than the initial hole radius. For biologically relevant values of the parameters (see Supporting Material), we expect  $\rho^2/\delta \ll 1$  but not negligibly small; this supports the assumption that the physical process of hole growth and healing is characterized by the hole-growth-dominated dynamics. In the other limit,  $\rho^2/\delta \gg 1$ , which is

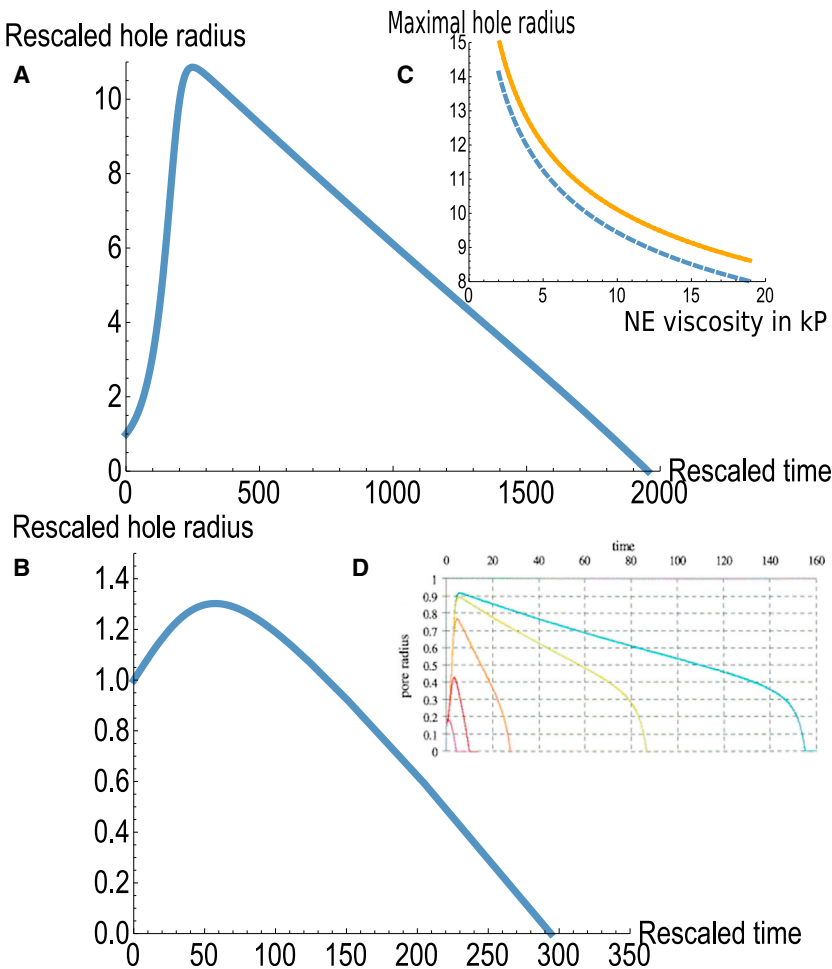


FIGURE 3 Rescaled hole radius  $R$  as a function of dimensionless time  $t$  for hole-growth-dominated (A) and outflow-dominated (B) dynamics. (C) This shows the maximal hole radius as a function of the shell viscosity numerically (dashed line) and analytically, using Eq. 9 (solid line). (D) Given here is the pore radius as a function of time in rescaled units for increasing inner fluid viscosity from left to right, taken from Brochard-Wyart et al. (28) with permission (fig. 2 in the reference). In (A–C), the time is rescaled by the viscoelastic timescale  $\tau = \eta/E$ , which is estimated to 20 s from the measurements of (10). To see this figure in color, go online.

characterized by either large initial holes or small effective dissipation length  $d^*$ , the dynamics of the hole radius are characterized by only a small increase of the hole radius that is quadratic in time. Our numerical analysis of the equations, shown in Fig. 3 B, shows that this generally leads to a small increase of the hole radius compared to its initial value before the line tension dominates the physics and the hole begins to shrink. A physical understanding of these two limits is as follows: when  $d^*$  is relatively small, the outflow occurs quickly, thus reducing the shell area and relaxing the surface tension induced by the deformation. The hole has then only a relatively short time to grow before the surface tension is reduced and the line tension dominates, causing the hole to shrink. In the other limit, the outflow is much slower and the surface tension is not quickly relaxed, thus permitting the hole to grow to much larger values before the surface tension is relieved and the line tension causes the hole to shrink.

For the purpose of fully characterizing the rupture dynamics (which affects the amount of polymer that extrudes through the hole) in addition to the early and late-time behaviors, one must consider the transition between these two regimes. We thus approximate (see Supporting Material)  $R(t)$  as a piecewise function of time, comprising different expressions for growth and healing, where the transition time between the two regimes is denoted by  $t_m$  at which the hole reaches its maximum size,  $R_m$ .

A closed-form for the maximal radius  $R_m$  is given by an expression that can be derived from the dynamical equations (see Supporting Material):

$$2\beta \int_0^{t_m} R^3 dt \approx 1 + \frac{\varepsilon_0 \delta}{\rho^2} - R_m^4. \quad (8)$$

For the case of hole-growth-driven strain-relief dynamics ( $(\delta/\rho^2) \gg 1$ ), we approximate the slope of the linear decrease regime to be  $-\beta/2$ , and find that (see Supporting Material)

$$R_m \approx \left( \frac{\varepsilon_0 \delta}{\rho^2} \right)^{\frac{1}{4}}, \quad (9)$$

which is in good agreement with the numerics for a wide range of shell surface viscosities, as shown in Fig. 3 C.

Equation 9 can be written in dimensional units as  $(\pi R_m^2/A_u) = (\varepsilon_0(\eta_s d^*/\eta))^{(1/2)}$ , which predicts the ratio of the maximal hole area and the shell undeformed area (for the fixed constriction cross-sectional area). This ratio increases as the square root of the initial strain  $\varepsilon_0$ , solvent kinematic viscosity  $\eta_s$ , and the effective dissipation length  $d^*$ . The value  $\varepsilon_0$  is the initial strain that drives hole growth, whereas the strain relief that limits hole growth decreases with increasing  $\eta_s$  or  $d^*$ , which limits the

outflow and promotes hole growth. The maximal radius also decreases with shell surface viscosity  $\eta$ , which slows the hole growth, thus allowing more strain relief by outflow.

### Case II: nucleoplasm as a homogenous viscous fluid

In this case, we coarse-grain the semiflexible polymer and solvent phases and model them both as a homogenous fluid with an effective, kinematic viscosity  $\eta_s^*$ , which is much higher than the kinematic viscosity of the solvent phase alone. In this model, the dissipation length corresponds to the actual thickness of the shell and is therefore typically smaller than the radius of the hole, particularly when the hole size approaches its maximum, the stage at which the outflow is highest and thus most important. This is in contrast to the former case in which  $d^*$  was much larger than the hole radius so that the end effects of the flow could be neglected. Here, the inner side of the shell forms a barrier to the flow, which causes bending of the flow lines except in the vicinity of the small hole; this results in an effective dissipation length proportional to  $R$ , which leads to a scaling law for  $Q$  of the form  $Q \sim \Delta p R^3/\eta_s$  (compared with  $Q \sim \Delta p R^4/(d^* \eta_s)$  in the former case); a detailed derivation can be found in section 4.29 of (47). This leads to a slightly modified set of equations, which are presented and discussed in the seminal article of the Brochard-Wyart group (28). These equations were solved numerically and analytically in the limit of high internal fluid kinematic viscosity, which is appropriate for the high value of the effective, kinematic viscosity of the solution in this model. The dynamics is characterized by an exponential growth of the hole size up to a maximal hole size, followed by an approximately linear decrease of the hole radius, with a velocity of  $(dR/dt) = -(8TdR_m/3\eta_s^*A_u)$  or  $(d\tilde{R}/d\tilde{t}) = -(8\beta\rho d/3\pi\delta)\tilde{R}_m$  in dimensionless form (where lengths are rescaled by  $R_i$ ). The final stage of hole closing is a fast regime with velocity of  $-T/2\eta$ , similar to the velocity as predicted in the former case (see Fig. 3 D).

However, in contrast to the similarities between the dynamics of case I and case II, the maximal hole radius  $R_m$  in case II is much larger than that predicted in case I. The ratio of the expressions for outflow of case II and I is  $(\eta_s d^*/\eta_s^* R)$  and can be very small if the effective, kinematic viscosity in case II is much larger than the kinematic viscosity of case I, especially for a large hole radius. This implies that the outflow  $Q$  in case II is much smaller and is actually negligible in the short, exponentially growing regime in the limit of a large effective, kinematic viscosity of the solution. This means that in this case, the maximal hole radius is the same as the metastable hole radius in flat, tensed membranes (26), and can be written for rescaled dimensionless parameters as (see Supporting Material):

$$R_m = \sqrt{\frac{\varepsilon_0}{\rho}} - \frac{\beta}{2\varepsilon_0}. \quad (10)$$



This is qualitatively different from case I, in which the outflow cannot be neglected in the hole growth regime and serves as a strain relief mechanism that impedes hole growth, leading to a maximal hole radius much smaller than the maximal hole radius of case II. An additional important characteristic of Eq. 10 is that, in contrast to Eq. 9 in the former model, Eq. 10 is independent of the viscoelastic properties of the shell.

Because the fast closing regime is characterized by a hole size that is relatively small, most of the outflow occurs in the slow, approximately linear closing regime (28). Therefore, the fast closing regime is not of any importance in our work; henceforth, we neglect this regime and focus on the slow, approximately linear, closing regime that is the rate-limiting step for hole closing. We shall see in the next subsection that the contribution to the amount of polymer that is extruded through the rupture is primarily determined by this regime.

### Polymer extrusion as a model for chromatin herniation

As long as the hole is open, there is a finite probability for a polymer to extrude through the hole. However, this requires the polymer to bend to a radius of curvature that is smaller than the size of the hole. For flow rates that are smaller than  $(k_B T / \eta_s) \approx 5 (\mu\text{m}^3/\text{s})$  (for solvent kinematic viscosity that is comparable to that of water), a condition that is satisfied in systems of biological relevance (see [Supporting Material](#)), the bending of the polymer chains is driven by thermal fluctuations (48,49). The rate  $v_e$  of chromatin escape can therefore be written as a sum of Boltzmann factors, and can be approximated by  $v_e = \nu_0 e^{-(\pi l_p / 2R)}$  (where  $\nu_0$  is an attempt frequency, and  $l_p$  is the persistence length of the semiflexible polymer), which represents the extrusion rate of a polymer chain that is bent to a radius of curvature equal to the maximal radius allowed, the hole radius  $R$ , by thermal fluctuation.

To estimate the total amount of polymer that extrudes during a hole growth/healing cycle, which is taken to be exponential growth up to maximal hole radius  $R_m$  followed by a linear decrease with a dimensionless, rescaled velocity of  $-\alpha$ , we integrate  $v_e$  over the entire cycle, which results in the dimensionless measure of the amount of extruded polymer  $L_c$  (see the [Supporting Material](#)):

$$L_c = \frac{\nu_0 \tau}{\alpha} R_m \left( e^{-\frac{\pi l_p}{2R_m}} + \frac{\pi l_p}{2R_m} \text{Ei} \left( -\frac{\pi l_p}{2R_m} \right) \right), \quad (11)$$

where  $\tau$  is the typical viscoelastic timescale  $\eta/E$  of the shell,  $\alpha = \beta/2$  for case I, which considers formation of a conduit; and  $\alpha = (8\beta\rho d / 3\pi\delta) R_m$  for the model of case II, where the entire polymer solution is treated as a high-viscosity, viscous fluid.

Equation 11 is correct for both models of the polymer solution rheology, even though the two models represent completely different approaches to model the complex hydrodynamics of the solution. We therefore conclude that Eq. 11 is universal in the sense that all models for the complex hydrodynamics of the solution will result in expressions of the form of Eq. 11, which differ in the dependences of  $\alpha$  and  $R_m$  on the model parameters. It is important to note that whereas  $\alpha$  appears in the expression for the amount of extruded polymer as a prefactor,  $R_m$  appears in the exponent; therefore, changes in  $R_m$  affect the amount of extruded polymer much more dramatically than changes of  $\alpha$ . This is expected, because the amount of extruded polymer scales linearly with the time that the hole is open, which in turn, approximately scales as  $\sim 1/\alpha$ , but scales exponentially with the bending energy required to bend the polymer, which scales as  $\sim 1/R_m$  for a maximally sized hole. This also explains why neglecting the fast closing regime of case II is reasonable; the fast closing regime occur for relatively small hole radii, where the amount of extruded polymer is exponentially smaller than the amount for hole radii around  $R_m$ . Thus, the amount of extruded polymer is more sensitive to the maximal hole size in the shell than to its closing velocity.

### DISCUSSION

We now relate our theory and its predictions to experimental observations of migration-induced rupture and damage. The theory does not depend on the details of the forces applied to the nucleus; what is important is the deformation of the NE that induces stretched, relatively high curvature regions. Thus, many of the results may be applicable to modes of deformation that cause blebbing and rupture other than migration, such as squeezing of the nucleus between two parallel surfaces (18). To apply the theory to these scenarios, the expression for the initial strain and the relation between viscoelastic properties of the NE and the lamins must be revised to account for the new geometry and deformation timescales.

In the scenario we consider, a hole in the lamina (even in the absence of one in the bilayer) is an essential first step that leads to bleb formation and inflation due to outflow, caused by the lack of mechanical force balance across the NE at the site of the laminar hole. The relatively high bending energy of the leading edge can promote nucleation of a hole in the lamina at the leading edge of the cell and nucleus; this prediction is consistent with the experimental observations of the frequent blebbing at the leading edge (8,14,15). We model the process by calculating the dynamics of hole growth and healing and polymer extrusion of a deformed viscoelastic shell that is filled with a high-concentration polymer solution in a good solvent. This model applies to a migrating nucleus where the lamina is treated as a viscoelastic layer and the chromatin as a

semiflexible polymer in a good solvent. Thus, our quantitative predictions focus on the dynamics of growth and healing in the lamina, which is coupled to outflow of fluid from the nucleus, through the hole and into the forming bleb. In addition, we estimate the amount of chromatin that herniates into the bleb as a function of the viscoelastic properties of lamina.

We now discuss possible biophysical implications of hole formation/healing, outflow, and chromatin herniation. These are not explicitly treated by our model but it is interesting to connect our viscoelastic hydrodynamics of the lamina to a possible interpretation of the subsequent processes of biological interest and observations. Although we do not explicitly treat bleb growth, our model is relevant because the growth is driven by outflow of fluid from the nucleoplasm through the lamina hole and into the bleb, eventually causing it to burst, which then transfers chromatin to the cytoplasm. This scenario suggests that the main cause of rupture-associated damage is exposure of chromatin to the cytoplasmic environment, which is biochemically different than the nucleoplasm and may promote chromatin damage. Therefore, the amount of extruded chromatin may correlate with chromatin damage. Of course, it is the bursting of the bleb, not the hole in the lamina, which causes the measured leakage of nucleoplasmic proteins to the cytoplasm; thus, our predictions of the lamina rupture dynamics should not be used to make predictions regarding the leakage of nucleoplasmic proteins, which is experimentally associated with rupture. The hole in the bleb may also heal due to competition between the line tension (which may be effectively augmented by the involvement of the ESCRT system) and the surface tension, which decreases over time due to outflow. We suppose that the time for the healing of holes in the viscoelastic lamina is much longer than the time of bleb formation and bursting. Therefore, we expect multiple cycles of bleb formation and bursting while the hole is open.

To date, experiments have presented qualitative evidence of NE rupture and/or loss of repair enzymes (based mainly on exchange of cytoplasmic and nucleoplasmic proteins), but not direct measurements of the dynamics of hole opening and closing (7,14,15,17). Different cells are characterized by different lamin expression levels and therefore different lamin content of their NE; these molecular-level differences can account for varying viscoelastic properties of the NE (10,11,37). The viscoelastic properties of the lamina control chromatin herniation and as a consequence, nuclear migration-induced damage. Qualitative indications of damage, such as the loss of survivability, chromatin herniation, or double-stranded breaks, were shown to increase with depletion of A-type lamins (8,14).

In addition to hole formation/healing, we have estimated in Eq. 11 the amount of chromatin that herniates through a hole in the lamina and into the bleb; if the bleb subsequently bursts, the chromatin can be transferred into the cytoplasm. Our estimate for herniation (Eq. 11) is presented as a closed

form expression depending on two parameters that characterize the dynamics of hole growth and healing: the maximal hole radius  $R_m$  and the approximately linear, closing velocity  $\alpha$ . The chromatin herniation is predicted to decrease with decreasing  $R_m$  or increasing  $\alpha$ . However, the contribution of the two do not affect the amount of herniated chromatin in the same manner: whereas the herniation decreases exponentially with  $R_m$ , it decreases only inversely with  $\alpha$ , which appears as a prefactor in Eq. 11. The parameters  $R_m$  and  $\alpha$  are determined by the line tension  $T$ , which is proportional to the 2D Young's modulus  $E$  (see Supporting Material), and the surface viscosity of the lamina  $\eta$ ; however, the exact dependence of  $R_m$  and  $\alpha$  on the viscoelastic parameters  $\eta$  and  $E$  is sensitive to the rheology of the nucleoplasm. In our model, we predict that  $R_m$  decreases with increasing  $\eta$  but is independent of  $E$ , whereas  $\alpha$  decreases with  $\eta$  and increases with  $E$ .

An increase of the lamina surface viscosity  $\eta$  slows the 2D flows within the lamina and retards hole growth. This retardation means that a relatively large amount of nucleoplasm can flow out of the hole leading to additional strain relief, compared with a system in which the hole grows quickly, so that the change of nuclear volume during hole growth is minimal. Thus, an increase of the surface viscosity of the lamina reduces the maximal hole radius, at least for case I of the rheology that we considered above. Because chromatin herniation is exponentially sensitive to the hole radius, our predicted decrease of  $R_m$  with increasing lamina surface viscosity (for one of the rheological models) means that increasing the laminar viscosity should greatly reduce the chromatin herniation.

Conversely, an increase of the 2D Young's modulus  $E$ , which controls the line tension responsible for hole closing, does not considerably modify the maximal hole radius. For large holes, the force due to line tension is inversely proportional to the hole radius and thus negligible compared with the surface tension. The line tension is thus relevant only after the surface tension becomes relaxed, at the hole closing regime. Indeed, in both models of the nuclear rheology the maximal hole radius is approximately independent of the line tension  $T$ . However, the line tension does affect the hole closing rate because the line tension is the driving force for the healing process. Indeed, the hole closing velocity,  $\alpha$ , increases with  $T$ . Thus, increasing the laminar elastic modulus,  $E$ , will lead to an increase of  $\alpha$  and to a decrease in the herniation of chromatin. In contrast to an increase in the laminar viscosity, which leads to a possibly exponential decrease of the herniation, an increase of  $E$  algebraically decreases the herniation because it enters through the prefactor and not the exponent.

Various experiments have measured the relative contributions of the different lamin subtypes to the viscoelastic properties of the NE. These experiments, which differed in the timescales and method of measurements, have been interpreted to ascribe differing contributions of A-type lamins

to the viscoelastic properties. In some experiments, A-type lamins were found to contribute primarily to the viscosity  $\eta$  (10,50), whereas in others it was found to contribute to the stiffness (11,37). Our predictions for chromatin herniation summarized here are cast in terms of the viscoelastic parameters and future experiments elucidating their molecular origins at the timescales appropriate to laminar hole formation/closing will enable further understanding at the molecular scale.

Returning to the focus of our theory, we suggest the following experiments. First, quantitative imaging of the lamina hole size as a function of the viscoelastic properties of the NE can distinguish between the two models we presented for the nucleoplasm rheology and determine which is more realistic. For example, measurements of the maximal hole radius  $R_m$ , as a function of the NE surface viscosity  $\eta$ , can distinguish the conduit model (case I) from the homogeneous viscous fluid model (case II), because Eq. 9 for case I predicts  $R_m \sim \eta^{-1/4}$ , whereas Eq. 10 for  $R_m$  (case II) is independent of  $\eta$ . Similar quantification can be done for the velocity of hole closing in regime where the velocity is approximately constant. In addition, quantification of chromatin herniation as a function of  $R_m$  or  $\alpha$ , by quantitative imaging of the hole size as a function of time, can test Eq. 11 for chromatin herniation. Quantification of the amount of chromatin that herniates through the hole as a function of the A-type lamin expression levels should also allow experiments to distinguish between the proposed contributions of type-A lamins to the viscoelastic properties of the lamina: if expression of type-A lamins mainly augments the viscosity, one might observe an exponential change of the chromatin herniation, whereas if it mainly augments the stiffness (through increasing  $E$ ), we predict a possibly weaker algebraic dependence.

## SUPPORTING MATERIAL

Supporting Materials and Methods are available at [http://www.biophysj.org/biophysj/supplemental/S0006-3495\(17\)30812-3](http://www.biophysj.org/biophysj/supplemental/S0006-3495(17)30812-3).

## AUTHOR CONTRIBUTIONS

D.D. performed research and wrote the article. D.E.D. designed research and contributed to the article. S.A.S. designed research and wrote the article.

## ACKNOWLEDGMENTS

The authors thank F. Brochard-Wyart, B. Berkowitz, J. Karni, R. Bar-Ziv, Y. Garini, M. Lenz, D. Ben-Yaakov, J. Irianto, C. Pfeifer, Y. Xia, K. Wolf, J. Lammerding, O. Cohen, and A. Moriel for the enlightening comments and useful discussions.

This work was funded by the U.S.-Israel Binational Science Foundation and the Israel Science Foundation, and was supported by the Schmidt Minerva Center and the Villalon Foundation. The historic generosity of the Perlman Family Foundation is also acknowledged.

## REFERENCES

- Li, G. W., and X. S. Xie. 2011. Central dogma at the single-molecule level in living cells. *Nature*. 475:308–315.
- Phillips, R., J. Kondev, ..., H. Garcia. 2012. *Physical Biology of the Cell*. Garland Science, New York.
- Alberts, B., A. Johnson, ..., P. Walter. 2002. *Molecular Biology of the Cell*. Garland Science, New York.
- Photos, P. J., H. Bermudez, ..., D. E. Discher. 2007. Nuclear pores and membrane holes: generic models for confined chains and entropic barriers in pore stabilization. *Soft Matter*. 3:364–371.
- Grossman, E., O. Medalia, and M. Zwerger. 2012. Functional architecture of the nuclear pore complex. *Annu. Rev. Biophys.* 41:557–584.
- Burke, B., and C. L. Stewart. 2014. Functional architecture of the cell's nucleus in development, aging, and disease. *Curr. Top. Dev. Biol.* 109:1–52.
- Irianto, J., R. Charlotte, ..., D. E. Discher. 2015. Constricted cell migration causes nuclear lamina damage, DNA breaks, and squeeze-out of repair factors. *bioRxiv*. <http://dx.doi.org/10.1101/035626>.
- Harada, T., J. Swift, ..., D. E. Discher. 2014. Nuclear lamin stiffness is a barrier to 3D migration, but softness can limit survival. *J. Cell Biol.* 204:669–682.
- Lammerding, J., P. C. Schulze, ..., R. T. Lee. 2004. Lamin A/C deficiency causes defective nuclear mechanics and mechanotransduction. *J. Clin. Invest.* 113:370–378.
- Swift, J., I. L. Ivanovska, ..., D. E. Discher. 2013. Nuclear lamin-A scales with tissue stiffness and enhances matrix-directed differentiation. *Science*. 341:1240104.
- Stephens, A. D., E. J. Banigan, ..., J. F. Marko. 2017. Chromatin and lamin A determine two different mechanical response regimes of the cell nucleus. *Mol. Biol. Cell*. 28:1984–1996.
- Christensen, R. 2012. *Theory of Viscoelasticity: An Introduction*. Elsevier, Dordrecht, Netherlands.
- Dahl, K. N., A. J. Engler, ..., D. E. Discher. 2005. Power-law rheology of isolated nuclei with deformation mapping of nuclear substructures. *Biophys. J.* 89:2855–2864.
- Denais, C. M., R. M. Gilbert, ..., J. Lammerding. 2016. Nuclear envelope rupture and repair during cancer cell migration. *Science*. 352:353–358.
- Raab, M., M. Gentili, ..., M. Piel. 2016. ESCRT III repairs nuclear envelope ruptures during cell migration to limit DNA damage and cell death. *Science*. 352:359–362.
- Irianto, J., C. R. Pfeifer, ..., D. E. Discher. 2016. Nuclear constriction segregates mobile nuclear proteins away from chromatin. *Mol. Biol. Cell*. 27:4011–4020.
- Robijns, J., F. Molenberghs, ..., T. D. J. Corne. 2016. In silico synchronization reveals regulators of nuclear ruptures in lamin A/C deficient model cells. *Sci. Rep.* 6:30325.
- Le Berre, M., J. Aubertin, and M. Piel. 2012. Fine control of nuclear confinement identifies a threshold deformation leading to lamina rupture and induction of specific genes. *Integr. Biol.* 4:1406–1414.
- Ryan, J., H. K. Petrie, and K. M. Yamada. 2014. Generation of compartmentalized pressure by a nuclear piston governs cell motility in a 3D matrix. *Science*. 345:1062–1065.
- Bennett, R. R., C. R. Pfeifer, ..., A. J. Liu. 2017. Elastic-fluid model for DNA damage and mutation from nuclear fluid segregation due to cell migration. *Biophys. J.* 112:2271–2279.
- Schroeder, A., J. Kost, and Y. Barenholz. 2009. Ultrasound, liposomes, and drug delivery: principles for using ultrasound to control the release of drugs from liposomes. *Chem. Phys. Lipids*. 162:1–16.
- Huang, H. W. 2006. Molecular mechanism of antimicrobial peptides: the origin of cooperativity. *Biochim. Biophys. Acta Biomembr.* 1758:1292–1302.
- Kozlovsky, Y., L. V. Chernomordik, and M. M. Kozlov. 2002. Lipid intermediates in membrane fusion: formation, structure, and decay of hemifusion diaphragm. *Biophys. J.* 83:2634–2651.

24. Smith, K. C., J. C. Neu, and W. Krassowska. 2004. Model of creation and evolution of stable electropores for DNA delivery. *Biophys. J.* 86:2813–2826.
25. Safran, S. A., and J. Klein. 1993. Surface instability of viscoelastic thin films. *J. Phys. II* 3:749–757.
26. Sens, P., and S. A. Safran. 1998. Pore formation and area exchange in tense membranes. *Eur. Phys. Lett.* 43:95.
27. Sandre, O., L. Moreaux, and F. Brochard-Wyart. 1999. Dynamics of transient pores in stretched vesicles. *Proc. Natl. Acad. Sci. USA* 96:10591–10596.
28. Brochard-Wyart, F., P. G. De Gennes, and O. Sandre. 2000. Transient pores in stretched vesicles: role of leak-out. *Phys. A* 278:32–51.
29. Levin, Y., and M. A. Idiart. 2004. Pore dynamics of osmotically stressed vesicles. *Phys. A* 331:571–578.
30. Idiart, M. A., and Y. Levin. 2004. Rupture of a liposomal vesicle. *Phys. Rev. E Stat. Nonlin. Soft Matter Phys.* 69:061922.
31. Ryham, R. J., F. S. Cohen, and R. S. Eisenberg. 2012. A dynamic model of open vesicles in fluids. *Commun. Math. Sci.* 10:1273–1285.
32. Ryham, R., I. Berezovik, and F. S. Cohen. 2011. Aqueous viscosity is the primary source of friction in lipidic pore dynamics. *Biophys. J.* 101:2929–2938.
33. Gozen, I., and P. Dommersnes. 2014. Pore dynamics in lipid membranes. *Eur. Phys. J. Spec. Top.* 223:1813–1829.
34. Fan, H., Y. Chen, and K. Y. Sze. 2009. Phenomenological modeling for pore opening, closure and rupture of the GUV membrane. *Int. J. Appl. Mech.* 1:327–338.
35. Bar-Ziv, R., E. Moses, and P. Nelson. 1998. Dynamic excitations in membranes induced by optical tweezers. *Biophys. J.* 75:294–320.
36. Bronshtein, I., I. Kanter, ..., Y. Garini. 2016. Exploring chromatin organization mechanisms through its dynamic properties. *Nucleus* 7:27–33.
37. Lammerding, J., L. G. Fong, and R. T. Lee. 2006. Lamins A and C but not lamin B1 regulate nuclear mechanics. *J. Biol. Chem.* 281:25768–25780.
38. Dahl, K. N., A. J. Ribeiro, and J. Lammerding. 2008. Nuclear shape, mechanics, and mechanotransduction. *Circ. Res.* 102:1307–1318.
39. Mitra, K., I. Ubarretxena-Belandia, ..., D. M. Engelman. 2004. Modulation of the bilayer thickness of exocytic pathway membranes by membrane proteins rather than cholesterol. *Proc. Natl. Acad. Sci. USA* 101:4083–4088.
40. Safran, S. A. 1994. *Statistical Thermodynamics of Surfaces, Interfaces, and Membranes*, Vol. 90. Perseus, New York.
41. Safran, S. A. 1999. Curvature elasticity of thin films. *Adv. Phys.* 48:395–448.
42. Landau, L. D., and E. M. Lifshitz. 1986. *Theory of Elasticity*, Vol. 7, Course of Theoretical Physics, 3. Butterworth-Heinemann, Oxford, UK, p. 109.
43. Turgay, Y., M. Eibauer, ..., O. Medalia. 2017. The molecular architecture of lamins in somatic cells. *Nature* 543:261–264.
44. Tseng, Y., J. S. Lee, ..., D. Wirtz. 2004. Micro-organization and viscoelasticity of the interphase nucleus revealed by particle nanotracking. *J. Cell Sci.* 117:2159–2167.
45. Bustamante, C., S. B. Smith, ..., D. Smith. 2000. Single-molecule studies of DNA mechanics. *Curr. Opin. Struct. Biol.* 10:279–285.
46. Neelam, S., T. J. Chancellor, ..., T. P. Lele. 2015. Direct force probe reveals the mechanics of nuclear homeostasis in the mammalian cell. *Proc. Natl. Acad. Sci. USA* 112:5720–5725.
47. Happel, J., and H. Brenner. 2012. *Low Reynolds Number Hydrodynamics: With Special Applications to Particulate Media*, Vol. 1. Springer Science & Business Media, New York.
48. Daoudi, S., and F. Brochard. 1978. Flows of flexible polymer solutions in pores. *Macromolecules* 11:751–758.
49. Béguin, L., B. Grassl, ..., H. Duval. 2011. Suction of hydrosoluble polymers into nanopores. *Soft Matter* 7:96–103.
50. Pajerowski, J. D., K. N. Dahl, ..., D. E. Discher. 2007. Physical plasticity of the nucleus in stem cell differentiation. *Proc. Natl. Acad. Sci. USA* 104:15619–15624.